

RELATIONS BETWEEN CENTRAL BLACK HOLE MASS AND TOTAL GALAXY STELLAR MASS IN THE LOCAL UNIVERSE

AMY E. REINES^{1,3} AND MARTA VOLONTERI²¹ Department of Astronomy, University of Michigan, 1085 South University Avenue, Ann Arbor, MI 48109, USA; reines@umich.edu² Institut d'Astrophysique de Paris, Sorbonne Universités, UPMC Univ Paris 6 et CNRS, UMR 7095, 98 bis bd Arago, F-75014 Paris, France
Received 2015 June 8; accepted 2015 August 24; published 2015 October 30

ABSTRACT

Scaling relations between central black hole (BH) mass and host galaxy properties are of fundamental importance to studies of BH and galaxy evolution throughout cosmic time. Here we investigate the relationship between BH mass and host galaxy total stellar mass using a sample of 262 broad-line active galactic nuclei (AGNs) in the nearby universe ($z < 0.055$), as well as 79 galaxies with dynamical BH masses. The vast majority of our AGN sample is constructed using Sloan Digital Sky Survey spectroscopy and searching for Seyfert-like narrow-line ratios and broad $H\alpha$ emission. BH masses are estimated using standard virial techniques. We also include a small number of dwarf galaxies with total stellar masses $M_{\text{stellar}} \lesssim 10^{9.5} M_{\odot}$ and a subsample of the reverberation-mapped AGNs. Total stellar masses of all 341 galaxies are calculated in the most consistent manner feasible using color-dependent mass-to-light ratios. We find a clear correlation between BH mass and total stellar mass for the AGN host galaxies, with $M_{\text{BH}} \propto M_{\text{stellar}}$, similar to that of early-type galaxies with dynamically detected BHs. However, the relation defined by the AGNs has a normalization that is lower by more than an order of magnitude, with a BH-to-total stellar mass fraction of $M_{\text{BH}}/M_{\text{stellar}} \sim 0.025\%$ across the stellar mass range $10^8 \leq M_{\text{stellar}}/M_{\odot} \leq 10^{12}$. This result has significant implications for studies at high redshift and cosmological simulations in which stellar bulges cannot be resolved.

Key words: galaxies: active – galaxies: evolution – galaxies: nuclei – galaxies: Seyfert

Supporting material: machine-readable tables

1. INTRODUCTION

A growing body of evidence suggests that supermassive black hole (BH) masses scale with the large-scale properties of their host galaxies, primarily of the bulge component (e.g., bulge mass, velocity dispersion, infrared luminosity; see, e.g., Magorrian et al. 1998; Ferrarese & Merritt 2000; Gebhardt et al. 2000a; Marconi & Hunt 2003; Häring & Rix 2004; Gültekin et al. 2009; Beifiori et al. 2012; Kormendy & Ho 2013; McConnell & Ma 2013, and references therein). These correlations on the one hand hint to a joint evolution of BHs and galaxies and contain crucial information on the cosmic assembly of structures; on the other hand, they provide a way to estimate BH masses via a proxy that is often much easier to measure. Extending these estimates to a statistical ensemble of galaxies allows one to eventually derive a census of BHs, such as their mass functions and total mass density locked into BHs (e.g., Marconi et al. 2004; Merloni 2004; Shankar et al. 2004, 2009; Gültekin et al. 2009; Kelly & Merloni 2012).

In the local universe, $z = 0$, benchmark BH masses are measured through direct methods, such as stellar and gas kinematics, and at the time of writing ~ 90 galaxies have dynamical BH masses (see Kormendy & Ho 2013; McConnell & Ma 2013; and <http://blackhole.berkeley.edu>). The masses of the bulges of the host galaxies can also be measured with good precision, using either photometric bulge/disk decomposition (e.g., Marconi & Hunt 2003) or kinematical fitting (Häring & Rix 2004) coupled with assumptions of the mass-to-light ratio (see Kormendy & Ho 2013, for a discussion).

Estimates of the relative mass of BHs and their host galaxies at higher redshift, which are of fundamental importance to

establish the timing of their growth, do not have access to the same wealth of information available locally. The BH masses are measured through indirect methods, and their uncertainties are discussed at length in the literature (e.g., Vestergaard & Peterson 2006; Shen 2013). The host properties are also estimated very differently. Except for gravitationally lensed galaxies (Peng et al. 2006) and/or *Hubble Space Telescope* images (Schramm & Silverman 2013; Park et al. 2015), which cannot provide a large statistical sample, reliable decomposition into the bulge and disk components are very difficult owing to the lack of spatial resolution and sensitivity (but see Sanghvi et al. 2014). Normally, the total stellar mass is used instead, estimated by assuming a mass-to-light ratio or spectral energy distribution (SED) fitting (e.g., Jahnke et al. 2009; Merloni 2010; Cisternas et al. 2011; Targett et al. 2012; Bongiorno et al. 2014; Sun et al. 2015), sometimes trying to select quasars with bulge-dominated host galaxies (Decarli et al. 2010) to lessen the discrepancy between bulge mass and total stellar mass. The scaling between BH and total stellar mass at high z is then often compared to the scaling between the BH and bulge mass at $z = 0$. Lauer et al. (2007) expose important biases incurred when investigating the potential evolution of BH scaling relations by comparing samples at different redshifts with different selection criteria (e.g., active galactic nucleus (AGN) activity versus host galaxy properties).

In this paper, we aim at quantifying on a local sample the difference between using total stellar mass and bulge stellar mass to calculate the BH-to-host relationship. While the tightest correlation appears to be the one between the BH and the bulge, we wish to provide a benchmark for high-redshift studies, which cannot avail themselves of bulge masses (or dynamical BH masses). We therefore investigate the

³ Hubble Fellow.

relationship between BH mass and total stellar mass in a large sample of nearby ($z \sim 0$) broad-line AGNs using techniques for estimating BH and galaxy masses similar to those used at $z > 0$. Making use of active BHs has the added advantage of extending our sample to the lowest-mass BHs known in galaxy nuclei (Reines et al. 2013; Baldassare et al. 2015).

2. SAMPLE OF BROAD-LINE AGNs

We construct our sample of broad-line AGNs by analyzing Sloan Digital Sky Survey (SDSS) spectra of $\sim 67,000$ emission-line galaxies and searching for objects exhibiting broad $H\alpha$ emission (signifying dense gas orbiting a massive BH), as well as narrow emission-line ratios indicating photoionization by an accreting massive BH. Our parent sample of emission-line galaxies is culled from the NASA-Sloan Atlas (NSA), which is based on the SDSS Data Release 8 (DR8) spectroscopic catalog (Aihara et al. 2011). While we use the NSA for selecting our parent sample of galaxies, we use our own software to analyze the SDSS spectra and search for broad-line AGNs. Distance estimates come from the `zdist` parameter in the NSA, which is based on the SDSS NSA redshift and the peculiar velocity model of Willick et al. (1997). We assume $H_0 = 70 \text{ km s}^{-1} \text{ Mpc}^{-1}$.

2.1. Parent Sample of Emission-line Galaxies

The NSA catalog of nearby galaxies ($z \leq 0.055$) provides a reanalysis of SDSS optical photometry using SDSS *ugriz* images with the improved background-subtraction technique described in Blanton et al. (2011). The NSA also provides a reanalysis of spectroscopic data from the SDSS using the methods described in Yan & Blanton (2012) and Yan (2011). We select emission-line galaxies in the NSA by imposing modest signal-to-noise ratio (S/N) cuts on emission-line measurements reported in the NSA. We require $S/N \geq 3$ for the flux and $S/N > 1$ for the EW of the $H\alpha$, [N II] $\lambda 6584$, and [O III] $\lambda 5007$ emission lines. We also require $S/N \geq 2$ for $H\beta$ and the [S II] $\lambda\lambda 6716, 6731$ doublet. This leaves us with a parent sample of 66,945 galaxies.

2.2. Spectral Analysis and Selection of Broad-line AGNs

We retrieved the SDSS spectra of our entire parent sample of galaxies and analyzed them with customized software that is described in detail in Reines et al. (2013) and briefly reviewed here for completeness. First, we model and remove the stellar continuum and absorption lines from the host galaxy using simple stellar population model templates spanning a range of ages and metallicities. Next, we model the narrow emission line profile based on the [S II] $\lambda\lambda 6716, 6731$ doublet. Once we have a suitable model of the [S II] doublet, we use it as a template for fitting the narrow emission lines in the $H\alpha + [\text{N II}] \lambda\lambda 6548, 6583$ complex. We fit the $H\alpha + [\text{N II}]$ complex twice, first with the narrow lines only and then allowing a broad $H\alpha$ component. We accept the fit with the broad $H\alpha$ component if statistically warranted (reduced χ^2 is improved by more than 50%⁴), and the FWHM of the broad $H\alpha$ component is $\geq 500 \text{ km s}^{-1}$ after correcting for the fiber-dependent instrumental resolution (e.g., see Figure 1). This FWHM requirement

avoids severe contamination from intensely star-forming galaxies with moderately broadened bases on $H\alpha$. We also measure fluxes of $H\beta$, [O III] $\lambda 5007$, and the [S II] doublet to place objects on standard narrow-line diagnostic diagrams (Baldwin et al. 1981; Veilleux & Osterbrock 1987; Kewley et al. 2001, 2006; Kauffmann et al. 2003).

Figure 2 shows the [O III]/ $H\beta$ versus [N II]/ $H\alpha$ and [O III]/ $H\beta$ versus [S II]/ $H\alpha$ narrow-line diagnostic diagrams for all objects with detectable broad $H\alpha$ emission. To minimize contamination from potential sources of broad $H\alpha$ other than ionized gas orbiting a BH (e.g., supernovae in star-forming galaxies and shocks in LINERs), we restrict our sample of broad-line AGNs to those sources falling in both the AGN region of the [O III]/ $H\beta$ versus [N II]/ $H\alpha$ diagram and the Seyfert region of the [O III]/ $H\beta$ versus [S II]/ $H\alpha$ diagram. We also visually inspect each individual object and cut sources with poor spectral fits (e.g., due to complicated line profiles including double-peaked lines) that may lead to erroneous BH masses based on broad $H\alpha$ (see below). A handful of objects are also excluded for reasons described in Section 2.4, leaving us with a final sample of 244 broad-line AGNs (Tables 1 and 2).

2.3. BH Masses and Luminosities

Single-epoch spectroscopic BH masses are routinely estimated for broad-line AGNs (e.g., Greene & Ho 2007b; Vestergaard & Osmer 2009; Schulze & Wisotzki 2010). Under the assumption that the broad-line region (BLR) kinematics are dominated by the gravity of the BH, the BH mass is given by $M_{\text{BH}} \propto R\Delta V^2/G$. The average gas velocity is inferred from the width of a broad emission line (typically $H\beta$), and the radius of the BLR is estimated from the radius–luminosity relation defined by reverberation-mapped AGNs (e.g., Kaspi et al. 2005; Bentz et al. 2013). The proportionality constant depends on the unknown geometry and orientation of the BLR. While these parameters have been seen to vary from object to object (Kollatschny 2003; Bentz et al. 2009; Denney et al. 2010; Barth et al. 2011), a single scaling factor is generally adopted from calibrating the ensemble of reverberation-based BH masses to the $M_{\text{BH}}-\sigma_*$ relation (e.g., Gebhardt et al. 2000b; Ferrarese et al. 2001; Nelson et al. 2004; Onken et al. 2004; Greene & Ho 2006; Park et al. 2012; Grier et al. 2013; Ho & Kim 2014).

We estimate BH masses for our sample of broad-line AGNs using the single-epoch virial mass estimator given by Equation (5) in Reines et al. (2013):

$$\log \left(\frac{M_{\text{BH}}}{M_{\odot}} \right) = \log \epsilon + 6.57 + 0.47 \log \left(\frac{L_{H\alpha}}{10^{42} \text{ erg s}^{-1}} \right) + 2.06 \log \left(\frac{\text{FWHM}_{H\alpha}}{10^3 \text{ km s}^{-1}} \right). \quad (1)$$

This equation was derived following the approach outlined in Greene & Ho (2005) for using the broad $H\alpha$ line, but incorporates the updated radius–luminosity relationship from Bentz et al. (2013). Here we adopt $\epsilon = 1.075$, corresponding to the mean virial factor $\langle f \rangle = 4.3$ from Grier et al. (2013), where $\epsilon = f/4$ (e.g., Onken et al. 2004). The distribution of BH masses for our sample of broad-line AGNs is shown in

⁴ Reines et al. (2013) used a threshold of 20% since they were focused on dwarf galaxies with low-mass BHs, which can have weak broad $H\alpha$ emission. Here we choose a higher threshold to help eliminate objects with marginally detected broad lines in higher-mass galaxies.

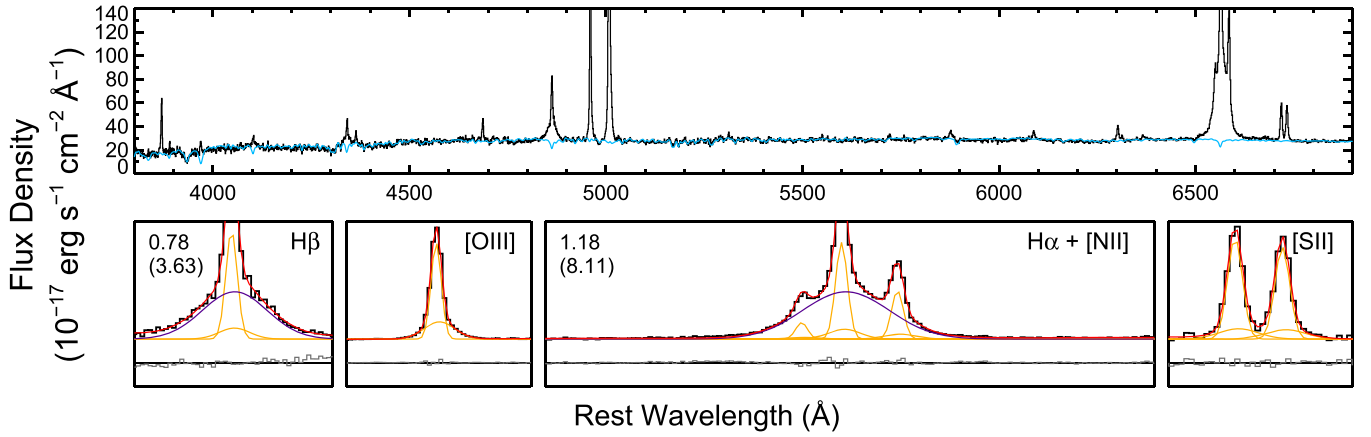


Figure 1. Spectrum of a broad-line AGN illustrating our fitting method. Top: the redshift-corrected spectrum is shown in black and the continuum plus absorption-line model is plotted in blue. Bottom: chunks of the emission-line spectrum (after subtracting the continuum and absorption-line model). The best-fit models for the emission-line regions are shown in red. The individual narrow-line Gaussian components are plotted in yellow. Broad $H\alpha$ and $H\beta$ Gaussian components are plotted in dark blue. The residuals are shown in gray with a vertical offset for clarity. In the upper left-hand corner of the $H\alpha$ and $H\beta$ chunks, we show the reduced χ^2 values from the fits *not* including a broad component for comparison.

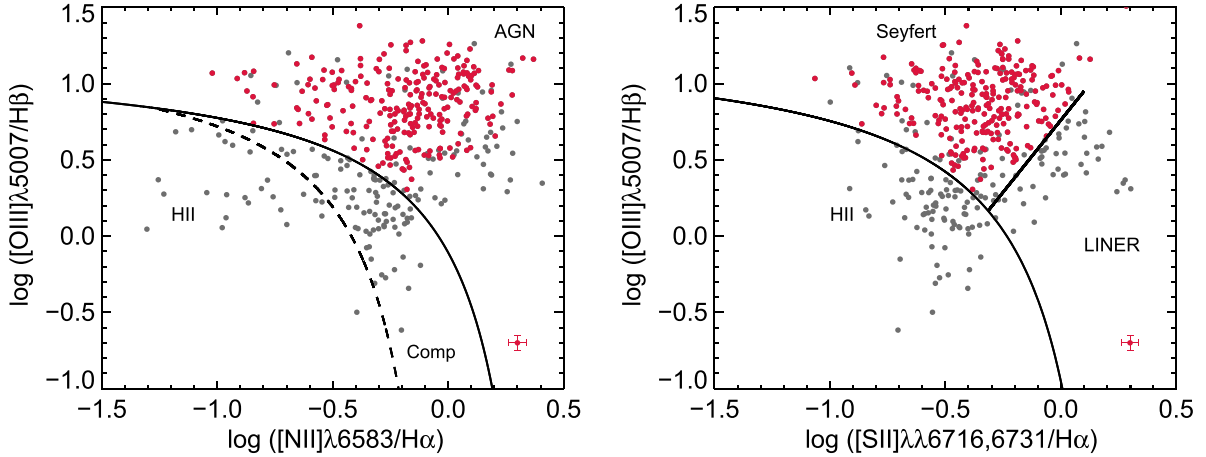


Figure 2. Narrow-line diagnostic diagrams for sources with detectable broad $H\alpha$ emission. We use the classification scheme outlined in Kewley et al. (2006). Our sample of broad-line AGNs is restricted to objects with narrow line ratios placing them in both the AGN region of the $[O\text{ III}]\lambda 5007/H\beta$ vs. $[N\text{ II}]\lambda 6583/H\alpha$ diagram and the Seyfert region of the $[O\text{ III}]\lambda 5007/H\beta$ vs. $[S\text{ II}]\lambda\lambda 6716,6731/H\alpha$ diagram (red points). The typical error for the red points is shown in the lower right corner of each plot.

Table 1
Sample of 244 Broad-line AGNs

ID (1)	NSAID (2)	SDSS Name (3)	Plate-MJD-Fiber (4)	zdist (5)	M_i (Host) (6)	$g - i$ (Host) (7)	$\log M_*$ (8)	$\log M_{\text{BH}}$ (9)
1	25955	J000907.90+142755.8	752-52251-320	0.0422	-21.81	1.06	10.68	6.2
2	22075	J004236.86-104922.0	655-52162-58	0.0424	-21.10	1.10	10.43	7.1
3	6452	J012159.81-010224.3	398-51789-10	0.0548	-22.77	0.49	10.47	7.7
4	23318	J021011.49-090335.5	667-52163-506	0.0419	-22.60	0.99	10.92	8.1
5	11183	J024912.86-081525.7	456-51910-77	0.0296	-20.64	0.96	10.11	5.7

Note. Column 1: identification number assigned in this paper. Column 2: NSA identification number. Column 3: SDSS name. Column 4: Plate-MJD-Fiber of analyzed spectra. Column 5: z_{dist} parameter in the NSA, which is based on the SDSS NSA redshift and the peculiar velocity model of Willick et al. (1997). Column 6: absolute i -band magnitude of the host galaxy. Column 7: $g - i$ color of the host galaxy. Magnitudes and colors have been corrected for foreground Galactic extinction (Schlegel et al. 1998), and the AGN contribution has been removed as described in Section 2.4. Column 8: \log host galaxy stellar mass in units of M_{\odot} , corrected for AGN contribution. Column 9: \log black hole mass in units of M_{\odot} . Uncertainties are on the order of 0.5 dex.

(This table is available in its entirety in machine-readable form.)

Figure 3. Viral BH mass estimates for broad-line AGNs are obviously very indirect and carry uncertainties of ~ 0.5 dex (e.g., Shen 2013).

We estimate the bolometric luminosities of the AGNs using the conversion between $L_{H\alpha}$ and L_{5100} given by Equation (1) in Greene & Ho (2005), where $L_{H\alpha}$ is the broad $H\alpha$ luminosity

and L_{5100} is the continuum luminosity at 5100 \AA , and $L_{\text{bol}} = 10.3 L_{5100}$ (Richards et al. 2006). The range of bolometric luminosities is $41.5 \lesssim \log L_{\text{bol}} \lesssim 44.4$ and the median is $\log L_{\text{bol}} \sim 43.4$, approximately 2.5 dex larger than the median of the distribution of broad $H\alpha$ luminosities (see Figure 3).

Table 2
Sample of 244 Broad-line AGNs: Emission-line Measurements

ID	(H β) _n	(H β) _b	[O III] λ 5007	[N II] λ 6548	(H α) _n	(H α) _b	[N II] λ 6583	[S II] λ 6716	[S II] λ 6731	FWHM (H α) _b
(1)	(2)	(3)	(4)	(5)	(6)	(7)	(8)	(9)	(10)	(11)
1	245(13)	...	1659(77)	301(13)	1192(31)	757(63)	892(39)	250(16)	219(11)	1501
2	481(26)	2343(147)	4960(87)	271(14)	2022(103)	11321(84)	803(24)	505(27)	417(29)	2121
3	664(47)	2073(289)	6841(203)	892(60)	3563(237)	16872(168)	2640(116)	627(53)	612(42)	3281
4	494(33)	...	1876(84)	761(49)	1802(116)	6309(715)	2252(150)	748(57)	585(69)	7720
5	32(5)	331(20)	296(20)	19(2)	176(15)	524(18)	57(5)	29(3)	28(3)	1081

Note. Column 1: identification number assigned in this paper. Columns 2–10: emission-line fluxes with units of 10^{-17} erg s $^{-1}$ cm $^{-2}$. Errors are given in parentheses. We have not applied an extinction correction. The subscripts n and b indicate the narrow and broad components of the line, respectively. A three-dot ellipsis indicates that no line was detected. Column 11: FWHM of the broad H α component.

(This table is available in its entirety in machine-readable form.)

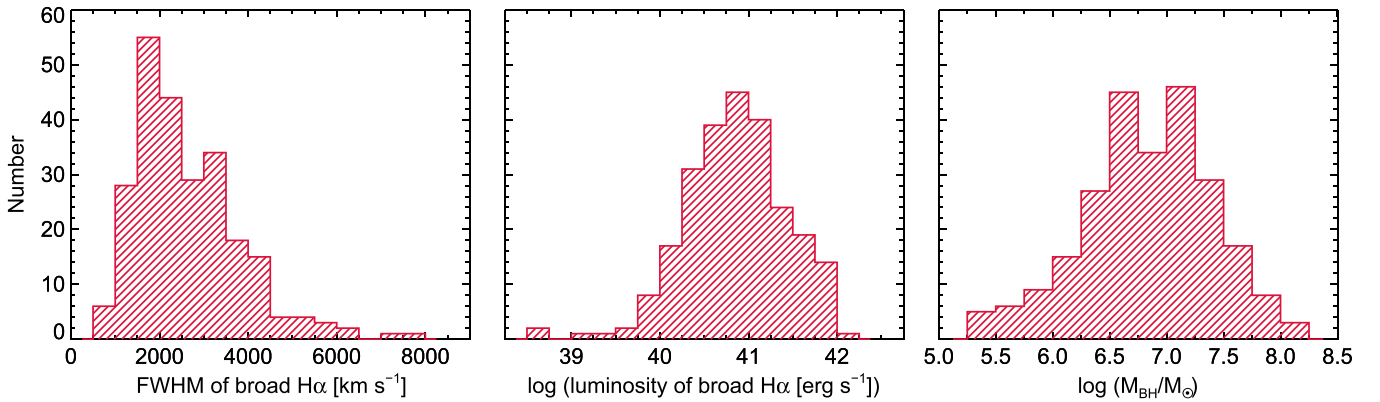


Figure 3. Distribution of the FWHM (left panel) and luminosity (middle panel) of broad H α emission for our sample of nearby broad-line AGNs. The distribution of virial BH masses calculated from Equation (1) is shown in the right panel.

2.4. Total Stellar Masses of the Host Galaxies

We estimate the total stellar masses, M_{stellar} , of galaxies hosting broad-line AGNs using mass-to-light ratios for i -band data (M/L_i) as a function of $g-i$ color following Zibetti et al. (2009), after removing the AGN contribution to the integrated photometry.

For each source, we estimate g -band and i -band flux densities of the AGN alone by constructing a mock AGN spectrum and convolving it with the SDSS filter throughput curves. The mock AGN spectrum consists of a power law ($f_\lambda \propto \lambda^\alpha$, where $\alpha = -1.56$ for $\lambda \leq 5000$ Å and $\alpha = -0.45$ for $\lambda > 5000$ Å; Vanden Berk et al. 2001) plus the observed strong emission lines measured from the SDSS spectrum (H β , [O III], H α , [N II], [S II]). We scale the mock AGN spectrum using the conversion between L_{5100} and $L_{\text{H}\alpha}$ (Greene & Ho 2005), where the broad H α luminosity is measured from the SDSS spectrum (Section 2.2). For the vast majority of our sample ($\sim 85\%$), the AGN contribution to the total g -band and i -band flux densities is less than 20% (see Figure 4). To minimize erroneous stellar mass estimates, we remove five sources from our sample in which the AGN dominates (i.e., contributes more than 50% to) the integrated flux densities.

After removing the AGN contribution, the host-only AB magnitudes (corrected for Galactic reddening) are used to estimate galaxy stellar masses with a color-dependent mass-to-light ratio from Zibetti et al. (2009):

$$\log(M/L_i) = 1.032(g - i) - 0.963. \quad (2)$$

We adopt a solar absolute i -band magnitude of 4.56 mag (Bell et al. 2003). Errors on the stellar masses are expected to be ~ 0.3 dex and are dominated by uncertainties in stellar evolution (Conroy et al. 2009).

In Figure 4, we compare total stellar masses of the host galaxies (with the AGN contribution removed) to those derived from the integrated photometry (without removing the AGN contribution). The median offset is 0.00 dex with a 1σ scatter of 0.04 dex. In some cases, the stellar mass actually increases slightly since the $g-i$ color gets redder once the (blue) AGN is removed, and a redder $g-i$ color increases M/L_i . The effect of correcting for AGN contamination is minimal since our sample is dominated by Seyferts of modest luminosity (Section 2.3). The distribution of stellar masses is shown in Figure 5.

We also compare the stellar masses of our sample based on the mass-to-light ratios in Zibetti et al. (2009) to those based on the mass-to-light ratios in Bell et al. (2003), as well as the stellar masses provided in the NSA based on SED fitting. For the Bell et al. (2003) masses, we again use M/L_i as a function of $g-i$ color. We then scale $\log M/L_i$ down by -0.093 dex (Gallazzi et al. 2008; Zibetti et al. 2009) to account for the differences between the Chabrier initial mass function (IMF) used in Zibetti et al. (2009) and the scaled Salpeter IMF used in Bell et al. (2003). The NSA stellar masses are derived from the `kcorrect` code (Blanton & Roweis 2007), which assumes a Chabrier IMF and fits broadband optical fluxes from the SDSS and ultraviolet fluxes from the *Galaxy Evolution Explorer* when available. Stellar masses from the three methods (using

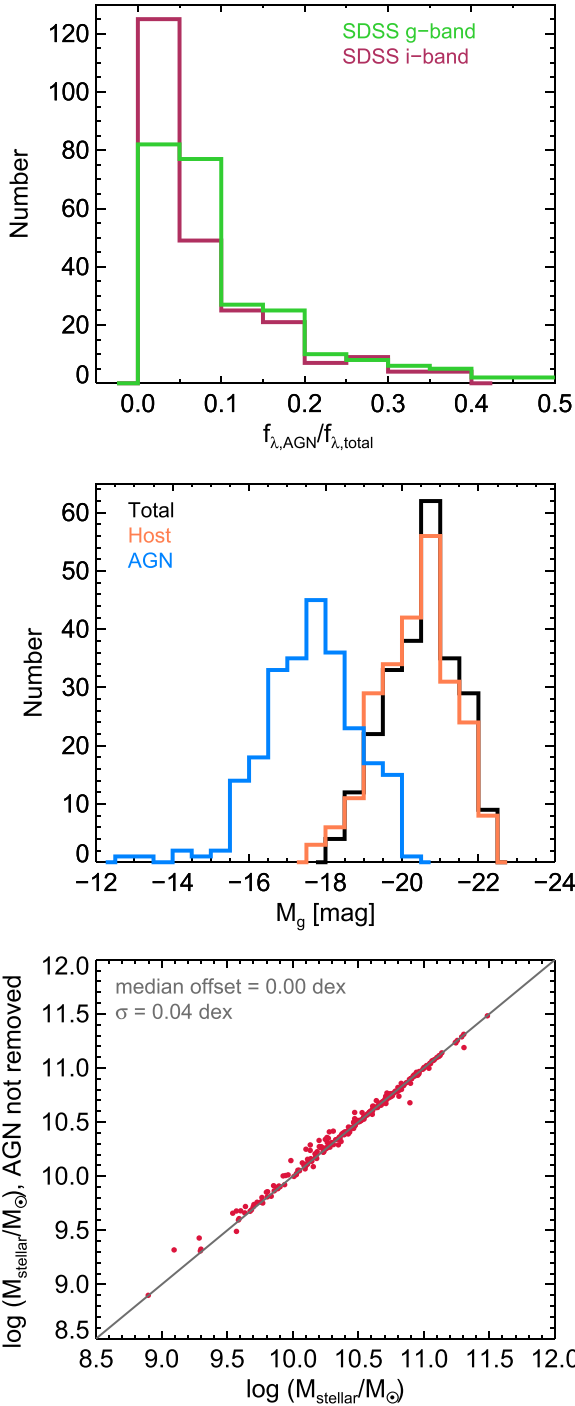


Figure 4. Top: distributions of the ratio of AGN flux density to total (Host +AGN) flux density in the SDSS *g* and *i* bands for our sample of broad-line AGNs. Middle: distributions of absolute *g*-band magnitudes for our sample of broad-line AGNs. The blue histogram shows AGN-only magnitudes, the orange histogram shows host-galaxy-only magnitudes, and the black histogram shows the total (Host+AGN) magnitudes. Bottom: total stellar mass without correcting for AGN contamination vs. total stellar mass corrected for AGN contamination. See Section 2.4 for details. The line shows the one-to-one relation.

integrated photometry in the NSA) are compared in Figure 6. The Bell et al. (2003) masses are systematically higher than the Zibetti et al. (2009) masses with a median offset of 0.21 dex ($\sigma = 0.10$ dex) across the sample, with the largest discrepancies

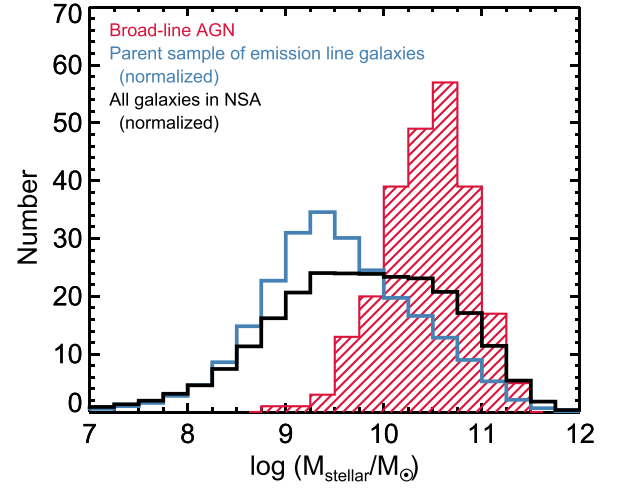


Figure 5. Distribution of host galaxy total stellar masses for our sample of broad-line AGNs (corrected for AGN contamination) is shown in red. Our parent sample of emission-line galaxies is shown in blue, normalized to the number of galaxies in the red histogram (244 objects). We also show the mass distribution for the full NSA catalog (no emission-line cuts), again normalized by the number of galaxies in the red histogram. All masses were derived using *g*- and *i*-band data in the NSA with the color-dependent mass-to-light ratio given in Equation (2).

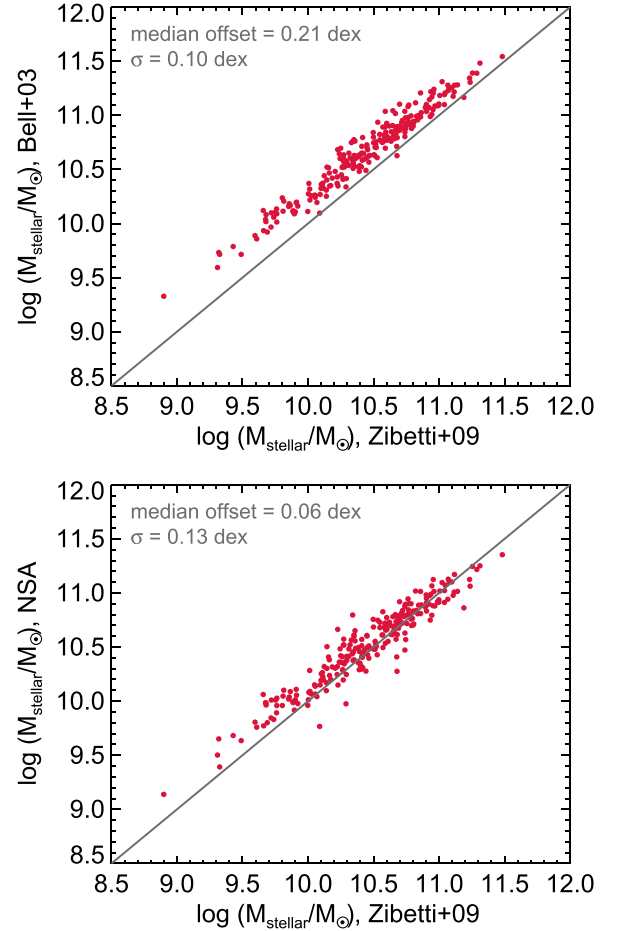


Figure 6. Comparison of stellar masses of our sample of broad-line AGNs derived from different methods. We calculate mass-to-light ratios for the SDSS *i*-band data as a function of *g* – *i* color following both Zibetti et al. (2009) and Bell et al. (2003) and using integrated photometry provided in the NSA (AGN contribution has not been removed). NSA masses are derived from the *kcorrect* code, which is described in detail in Blanton & Roweis (2007). The lines show the one-to-one relation.

at low masses. The NSA (`kcorrect`) masses are more consistent with the Zibetti et al. (2009) masses with a median offset of 0.06 dex ($\sigma = 0.13$ dex).

3. ADDITIONAL OBJECTS

We include the following additional objects in our investigation of the relationship between BH mass and host galaxy total stellar mass.

3.1. Dwarf Galaxies Hosting Broad-line AGNs

Reines et al. (2013) carried out the first systematic search for AGNs in dwarf galaxies. The vast majority of objects in that sample are narrow-line AGNs and composites as defined by Kewley et al. (2006), for which we have no estimates of the BH masses. However, 10 out of 136 AGNs and composite objects have detectable broad $H\alpha$ emission and narrow-line signatures suggesting the presence of an active BH (6 AGNs and 4 composites). This subsample includes the well-studied dwarf disk galaxy NGC 4395 hosting a Seyfert 1 nucleus (Filippenko & Sargent 1989; Filippenko & Ho 2003), two objects from the Greene & Ho (2007a) sample of low-mass BHs, and the dwarf disk galaxy presented in Dong et al. (2007). Reines et al. (2013) also provide information on 15 galaxies with broad $H\alpha$ emission, but narrow-line ratios dominated by star formation. As described in that work, there is likely significant contamination from luminous SNe II in that subsample, and we therefore do not include those objects here. This issue will be further addressed in a forthcoming paper (V. F. Baldassare et al. 2015, in preparation). BH masses and total stellar masses for the 10 broad-line AGNs and composites from Reines et al. (2013) are recomputed⁵ here in the same way as our full sample of broad-line AGNs (see Sections 2.3 and 2.4) and listed in Table 3.

We note that three of the broad-line objects from Reines et al. (2013) are also included in our main sample of broad-line AGNs in this work (including NGC 4395). The remaining seven objects are not recovered owing to different selection criteria. In this work, we exclude composite objects and also impose a more stringent threshold for flagging a source as having broad $H\alpha$ emission (see Section 2.2), since we are more concerned with having a clean sample than finding rare objects. In contrast, Reines et al. (2013) focused on finding low-mass BHs that can have weak broad $H\alpha$ emission in dwarf galaxies that tend to have more active star formation.

Follow-up high-resolution spectroscopy of the Reines et al. (2013) sample has led to the discovery of a new broad-line object with $M_{\text{BH}} \sim 50,000 M_{\odot}$ (Baldassare et al. 2015). This object, designated RGG 118 (object ID 118 in the Reines et al. paper), has the smallest BH reported in a galaxy nucleus. The BH mass for RGG 118 was estimated using Equation (1), and here we estimate the stellar mass of RGG 118 to be $M_{\text{stellar}} \sim 2.7 \times 10^9 M_{\odot}$ using the SDSS *i*- and *g*-band photometry in the NSA with Equation (2).

We also include the well-studied dwarf Seyfert 1 galaxy Pox 52 (Barth et al. 2004; Thornton et al. 2008). The mass of the BH in Pox 52 is $M_{\text{BH}} \sim 3 \times 10^5 M_{\odot}$ (Thornton et al. 2008). As Pox 52 is not in the SDSS footprint, we estimate the galaxy stellar mass using *B*-, *V*-, and *K*-band photometry (corrected for

⁵ Here we use $\epsilon = 1.075$ in Equation (1), rather than $\epsilon = 1$ as in Reines et al. (2013). Stellar masses are computed using Equation (2) rather than taken from the NSA as in Reines et al. (2013).

Table 3
Additional Objects

Name (1)	$\log M_{\star}$ (2)	$\log M_{\text{BH}}$ (3)
Dwarf Galaxies with Broad-line AGNs		
RGG 1	9.30	5.44(0.50)
RGG 9	9.24	5.00(0.50)
RGG 11	9.30	5.29(0.50)
RGG 20	9.29	6.10(0.50)
RGG 21	9.45	5.80(0.50)
RGG 32	8.90	5.28(0.50)
RGG 48	8.96	5.18(0.50)
RGG 118 ^a	9.43	4.70(0.50)
RGG 119	9.12	5.42(0.50)
RGG 123	9.36	5.79(0.50)
RGG 127	9.36	5.21(0.50)
Pox 52 ^b	8.63	5.48(0.50)
Reverberation-mapped AGNs		
Mrk 590	11.38	7.57(0.07)
Mrk 79	10.41	7.61(0.12)
Mrk 110	10.14	7.29(0.10)
NGC 3227	10.36	6.77(0.10)
SBS 1116+583A	10.00	6.56(0.08)
Arp 151	9.90	6.67(0.05)
Mrk 1310	9.62	6.21(0.08)
NGC 4051	10.16	6.13(0.14)
Mrk 202	9.92	6.13(0.17)
NGC 4253	10.34	6.82(0.05)
NGC 4395	8.90	5.45(0.14)
NGC 5273	10.25	6.66(0.16)
NGC 5548	10.79	7.72(0.02)
Mrk 817	9.87	7.59(0.07)
Mrk 290	9.52	7.28(0.06)
Galaxies with Dynamical BH Masses		
M32	8.77	6.39(0.18)
NGC 1316	11.48	8.23(0.07)
NGC 1332	10.92	9.17(0.06)
NGC 1374	10.33	8.77(0.04)
NGC 1399	11.17	8.94(0.33)
NGC 1407	11.43	9.67(0.05)
NGC 1550	11.02	9.59(0.07)
NGC 2960	10.72	7.03(0.02)
NGC 3091	11.29	9.57(0.04)
NGC 3377	10.14	8.25(0.23)

Note. Column 1: object name. Dwarf galaxies with the designation RGG are from Reines et al. (2013). Column 2: \log host galaxy stellar mass in units of M_{\odot} . The AGN contribution has been removed for the dwarf galaxies and reverberation-mapped AGNs. All stellar masses are estimated using color-dependent mass-to-light ratios from Zibetti et al. (2009). Uncertainties are on the order of 0.3 dex. Column 3: \log black hole mass in units of M_{\odot} . BH masses for the reverberation-mapped AGNs are taken from the AGN Black Hole Mass Database (Bentz & Katz 2015). Dynamical BH masses are taken from Kormendy & Ho (2013).

^a BH mass from Baldassare et al. (2015).

^b BH mass from Thornton et al. (2008).

(This table is available in its entirety in machine-readable form.)

the AGN contribution) provided by Barth et al. (2004) and Thornton et al. (2008) with the following color-dependent mass-to-light ratio from Zibetti et al. (2009):

$$\log(M/L_K) = 1.176(B - V) - 1.390. \quad (3)$$

We adopt a solar absolute K -band magnitude of 3.32 mag (Bell et al. 2003). The resulting stellar mass for Pox 52 is $M_{\text{stellar}} \sim 4.3 \times 10^8 M_{\odot}$. This is ~ 2.8 times smaller than the stellar mass estimated by Thornton et al. (2008) using the `kcorrect` code of Blanton & Roweis (2007). We adopt the Zibetti et al. (2009) mass for consistency with the rest of our sample.

As with our main sample of broad-line AGNs (Section 2), we adopt uncertainties of 0.3 dex in stellar mass and 0.5 dex in BH mass for all of the dwarf galaxies discussed above. However, we caution that the virial BH masses derived for these objects are based on an extrapolation from more massive and luminous AGNs and may carry additional errors. We do not include the dwarf galaxies Henize 2–10 (Reines et al. 2011; Reines & Deller 2012), Mrk 709 (Reines et al. 2014), or J1329+3234 (Secrest et al. 2015) since the BH masses in these systems are uncertain by at least an order of magnitude.

It is worth noting here that optical searches for AGNs in dwarf galaxies suffer from severe selection effects. First, low-metallicity AGNs, which are likely to reside in low-mass galaxies, have line ratios that are significantly different from Seyferts in more metal-rich systems and overlap with low-metallicity starbursts in the $[\text{O III}]/\text{H}\beta$ versus $[\text{N II}]/\text{H}\alpha$ (i.e., BPT) diagram (Groves et al. 2006; Kewley et al. 2013; Reines et al. 2014). Moreover, broad $\text{H}\alpha$ from small accreting BHs can be very weak and difficult to detect. Given the sensitivity of the SDSS spectra and our search volume ($z < 0.055$), Reines et al. (2013) estimate a minimum detectable BH mass of $M_{\text{BH}} \sim 10^5 M_{\odot}$ if the BH is radiating at $\sim 10\%$ of its Eddington limit.

3.2. Reverberation-mapped AGNs

The most reliable AGN BH masses come from reverberation mapping (e.g., Peterson et al. 2004; Bentz et al. 2009; Denney et al. 2010; Barth et al. 2011). Determining the time lag between the continuum flux and broad emission line variability gives the light-travel time across the BLR, and in turn the BLR radius when multiplied by the speed of light. The BLR radius–luminosity correlation derived from the sample of reverberation-mapped AGNs (~ 50 objects) makes single-epoch virial BH masses for AGNs, such as the ones used in this work, possible (e.g., Kaspi et al. 2005; Bentz et al. 2013). The reverberation-mapped AGNs also provide a link between single-epoch spectroscopic BH masses and dynamical BH masses, as the ensemble of reverberation-mapped BH masses is calibrated to the $M_{\text{BH}}-\sigma_*$ relation (e.g., Gebhardt et al. 2000b; Ferrarese et al. 2001; Nelson et al. 2004; Onken et al. 2004; Greene & Ho 2006; Park et al. 2012; Grier et al. 2013; Ho & Kim 2014).

In this work, we include 15 reverberation-mapped AGNs with BH masses provided in the AGN BH Mass Database (Bentz & Katz 2015). We adopt BH masses calculated with a mean virial factor of $\langle f \rangle = 4.3$ (Grier et al. 2013) as we did for the single-epoch spectroscopic masses given by Equation (1). We first cross-match the AGN BH Mass Database with the NSA and find 19 matches. We require that galaxies have photometry in the NSA so we can calculate the host galaxy stellar masses consistently with the rest of our AGN sample (Equation (2)). We correct for the AGN contribution to the integrated photometry, assuming the same power-law shape described in Section 2.4. However, for most of the reverberation-mapped AGNs, the normalization comes directly from L_{5100} provided in the AGN BH Mass Database. There are a few

cases where L_{5100} is not available, yet we have a measurement of broad $\text{H}\alpha$ from the SDSS spectrum. For these, we normalize the AGN continuum as described in Section 2.4. Emission lines are not included in the mock AGN spectrum for the reverberation-mapped AGNs because these measurements are not readily available in many cases. We exclude four objects (from the initial 19 matches) in which the AGN dominates the integrated photometry to minimize unreliable stellar mass estimates. BH masses and total stellar masses for the 15 reverberation-mapped AGNs used in this work are listed in Table 3.

We note that six of the reverberation-mapped AGNs in Table 3 are included in our main sample of broad-line AGNs with SDSS spectroscopy. As a consistency check, we compare the reverberation-mapped BH masses and those based on broad $\text{H}\alpha$ emission measured from the SDSS spectra (Equation (1)). For this limited sample of six objects, the spectroscopic BH masses are on average ~ 0.4 dex larger than the reverberation masses.

3.3. Galaxies with Dynamically Detected BHs

Benchmark BH masses come from dynamical methods, which rely on observations that spatially resolve the BH sphere of influence. Kormendy & Ho (2013) provide an inventory of BH mass measurements based on stellar dynamics, ionized gas dynamics, CO molecular gas disk dynamics, and maser disk dynamics.

We estimate total stellar masses of galaxies with dynamical BH mass measurements using the total absolute K -band magnitudes and $B - V$ colors provided by Kormendy & Ho (2013) in their Tables 2 and 3 with the color-dependent mass-to-light ratio from Zibetti et al. (2009) given in Equation (3) above. The results are listed in Table 3. We include all objects summarized in Kormendy & Ho (2013) except those with BH mass upper limits (two elliptical galaxies and two spiral galaxies with pseudobulges), and galaxies without provided $B - V$ colors that are necessary for estimating the galaxy stellar masses (two elliptical galaxies⁶ and three spiral galaxies with pseudobulges).

Kormendy & Ho (2013) provide a different way to predict M/L_K as a function of $B - V$ color (their Equation (9)). This relation is based on the mass-to-light ratio calibrations of Into & Portinari (2013), shifted to a dynamically measured zero point. Using Equation (9) in Kormendy & Ho (2013) yields stellar masses that are systematically higher than the Zibetti et al. (2009) masses by ~ 0.33 dex (see Figure 7). This discrepancy is primarily due to different assumed stellar IMFs in the models and the shift of 0.1258 dex in $\log M/L_K$ applied by Kormendy & Ho (2013). Zibetti et al. (2009) adopt a Chabrier IMF, whereas Into & Portinari (2013) assume a Kroupa IMF. The stellar IMF is known to significantly affect the overall normalization of $\log M/L_K$ (e.g., Bell & de Jong 2001). Here we adopt the Zibetti et al. (2009) masses for consistency with the other samples in this work.

⁶ Two additional elliptical galaxies do not have $B - V$ colors provided by Kormendy & Ho (2013); however, they do have M_{bulge} , which is equivalent to total stellar mass since these are ellipticals. We include these galaxies in our sample and adopt a total stellar mass $\log M_{\text{stellar}} = \log M_{\text{bulge}} - 0.33$, where the offset accounts for differences in our assumed mass-to-light ratios.

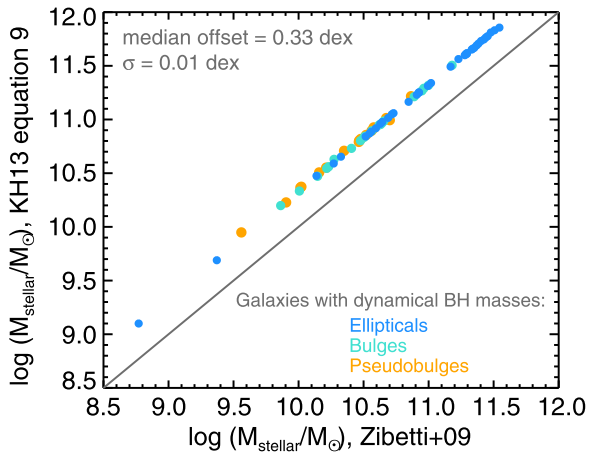


Figure 7. Total stellar masses of galaxies with dynamically measured BH masses derived using K -band mass-to-light ratios as a function of $B - V$ color from Equation (9) in Kormendy & Ho (2013) vs. Equation (3) here taken from Zibetti et al. (2009).

4. LOCAL BH MASS—TOTAL STELLAR MASS RELATIONS

One of the most useful aspects of BH-galaxy scaling relationships is that they provide a way to estimate BH mass from more easily measured galaxy properties. While the tightest scaling relations appear to be between the BH mass and bulge properties in quiescent early-type galaxies, we seek to quantify the relationship between BH mass and total stellar mass to facilitate work at higher redshifts where measuring bulge properties is difficult or impossible and BHs are identified via nuclear activity.

In Figure 8, we plot BH mass versus host galaxy total stellar mass for our local sample of 244 broad-line AGNs and the additional objects described in Section 3. A single linear relation is disfavored by the data. There is a large range in BH mass at a given total stellar mass (e.g., a factor of ~ 1000 in M_{BH} at $M_{\text{stellar}} \sim 10^{10.5} M_{\odot}$).

Despite a significant amount of scatter in this plot, it is clear that at a given total stellar mass, AGN host galaxies at $z \sim 0$ tend to fall below elliptical galaxies and spiral/S0 galaxies with classical bulges hosting quiescent BHs. If the spectroscopic BH masses were shifted down (see Section 3.2), this would cause an even larger discrepancy between the AGNs and the dynamically detected BHs in Figure 8. Similarly, the AGN host galaxies fall below the canonical BH-to-bulge mass relations defined by these inactive early-type galaxies (e.g., Häring & Rix 2004; Kormendy & Ho 2013; McConnell & Ma 2013). BHs in galaxies with pseudobulges also preferentially lie below the scaling relations based on ellipticals and classical bulges (also see Greene et al. 2010; Kormendy et al. 2011).

We note that bulge mass and total stellar mass are equivalent for elliptical galaxies, which dominate the samples used to derive BH-to-bulge mass relations. Indeed, we find that a linear regression using total stellar mass for the elliptical galaxies and spiral/S0 galaxies with classical bulges, which have dynamically measured BH masses (Section 3.3), is roughly consistent with standard bulge mass relations, albeit with more scatter (see below).

Thus, it appears that a separation exists between our sample of uniformly selected AGN hosts (Section 2) and ellipticals and classical bulges. We anticipate that using or extrapolating the canonical BH-to-bulge mass scaling relations to interpret

samples of galaxies with uncertain morphological classification, or AGN hosts, may lead to erroneous inferences.

4.1. The BH-to-total Stellar Mass Relation for Local AGNs

We plot $\log M_{\text{BH}}$ versus $\log M_{\text{stellar}}$ for the AGNs alone in the left panel of Figure 9. We first use a non-parametric method to help visualize the data and demonstrate that there is indeed a correlation between BH mass and total stellar mass for local AGNs. We use the kernel density estimation technique (e.g., Silverman 1986) to estimate the density function in the $\log M_{\text{stellar}} - \log M_{\text{BH}}$ plane from the observed data for all AGNs.⁷ Each data point is represented by a two-dimensional normalized Gaussian kernel. The smoothing parameter (e.g., σ for a Gaussian) is set to 0.3 and 0.5 for $\log M_{\text{stellar}}$ and $\log M_{\text{BH}}$, respectively, and reflects the measurement uncertainties for the majority of our sample (where masses are in units of M_{\odot}). The individual kernels are then summed to produce the kernel density estimate (left panel of Figure 9). The kernel density estimate is subsequently normalized for each $\log M_{\text{stellar}}$ independently to construct the conditional probability distribution function (PDF), $p(\log M_{\text{BH}} | \log M_{\text{stellar}})$, which illustrates the dependence of BH mass on total stellar mass for our sample of AGNs. The right panel of Figure 9 shows the resulting PDF, where the lines correspond to the median and standard deviation as a function of $\log M_{\text{stellar}}$.

This non-parametric method nicely illustrates a correlation between $\log M_{\text{BH}}$ and $\log M_{\text{stellar}}$ for our sample of AGNs. However, the shape/slope of the relation may be different for the *population* of local AGNs since the conditional PDF is based on data that are susceptible to selection biases that are particularly severe at low masses (see Section 3.1). While we should not immediately assume that these data are well described by a linear relation, the sample Pearson correlation coefficient indicates that a linear relationship between $\log M_{\text{BH}}$ and $\log M_{\text{stellar}}$ is a reasonable description of the data; $r = 0.54$ with a probability $p < 10^{-6}$ that no linear correlation is present. We therefore use a line to parameterize the AGN relation.

We take a Bayesian approach to linear regression using the method of Kelly (2007),⁸ which accounts for uncertainties in both $\log M_{\text{BH}}$ and $\log M_{\text{stellar}}$. To facilitate comparison with other studies, we parameterize the relation as

$$\log(M_{\text{BH}}/M_{\odot}) = \alpha + \beta \log(M_{\text{stellar}}/10^{11}M_{\odot}) \quad (4)$$

and find

$$\alpha = 7.45 \pm 0.08; \beta = 1.05 \pm 0.11. \quad (5)$$

The quoted slope and intercept are given by the median of 10,000 draws from the posterior probability distribution of the parameters. The errors on the linear coefficients are correlated and the reported values are determined from the 1σ error ellipse. The rms deviation of the BH mass measurements from the relation is 0.55 dex and incorporates both our adopted measurement errors of 0.50 dex and a best-fit intrinsic scatter of 0.24 dex (added in quadrature). The intrinsic scatter may be larger if our measurement errors are overestimated. The linear relation for the AGN host galaxies is shown in the left panel of Figure 10. We note that our results do not change significantly

⁷ For individual AGNs with multiple BH mass estimates, we include only one data point with priority given to reverberation masses when available (e.g., NGC 4395).

⁸ `linmix_err.pro` in the IDL Astronomy User's Library.

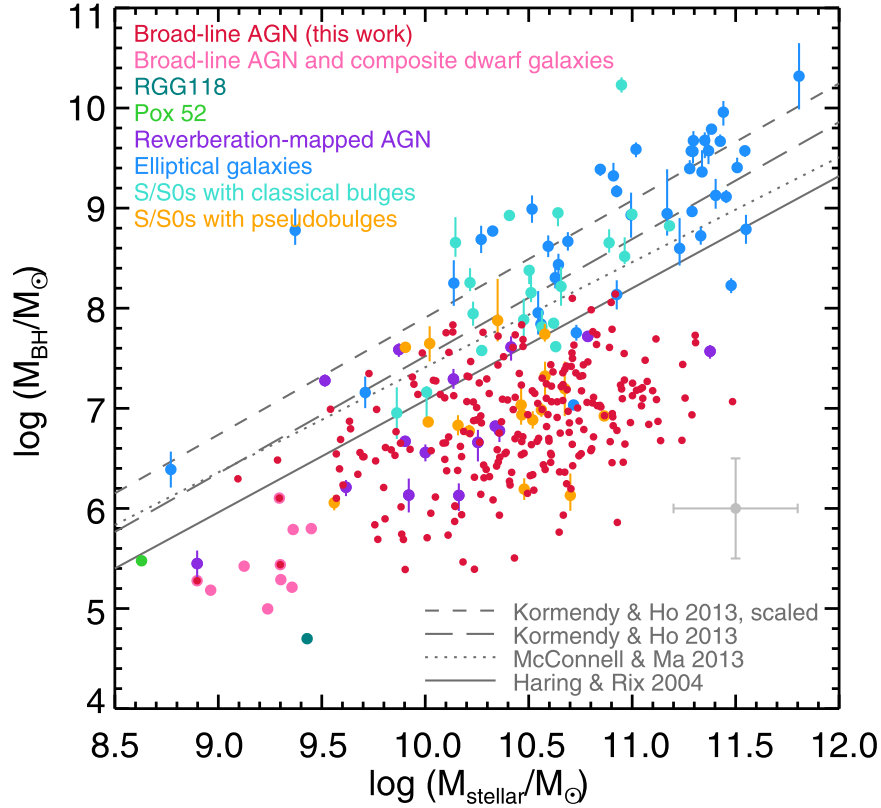


Figure 8. Left: black hole mass vs. total host galaxy stellar mass. All stellar masses are estimated using color-dependent mass-to-light ratios presented in Zibetti et al. (2009; see Sections 2.4 and 3). Our sample of 244 broad-line AGNs for which we estimate virial BH masses from Equation (1) are shown as red points. The 10 broad-line AGNs and composite dwarf galaxies from Reines et al. (2013) are shown as pink points (including NGC 4395; Filippenko & Sargent 1989). The dwarf galaxy RGG 118 (Reines et al. 2013) hosting a $\sim 50,000 M_{\odot}$ BH (Baldassare et al. 2015) is the dark green point, and Pox 52 (Barth et al. 2004; Thornton et al. 2008) is the light green point (see Section 3.1). Fifteen reverberation-mapped AGNs with BH masses taken from Bentz & Katz (2015) are shown as purple points (see Section 3.2). Dynamical BH mass measurements are taken from Kormendy & Ho (2013) and shown as blue (elliptical galaxies), turquoise (S/S0 galaxies with classical bulges), and orange (S/S0 galaxies with pseudobulges) points. The gray error bar indicates uncertainties in stellar masses for all points, and single-epoch spectroscopic BH masses. The gray lines show various M_{BH} vs. M_{bulge} relations based on ellipticals and spiral bulges with dynamical BH mass measurements. The Kormendy & Ho (2013) “scaled” relation has bulge masses scaled down by 0.33 dex to account for differences in our assumed mass-to-light ratios (see Section 3.3).

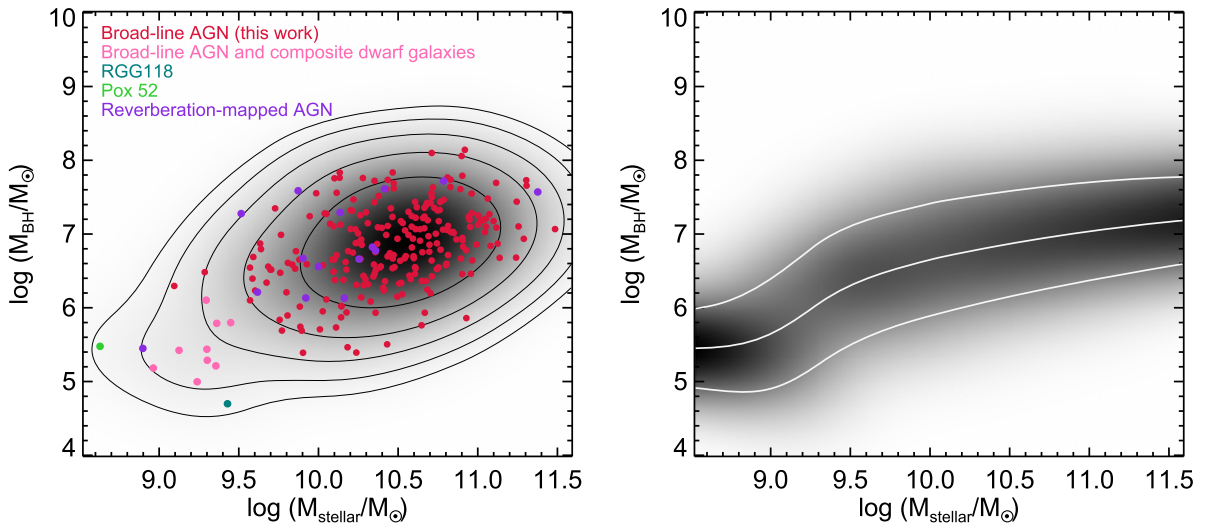


Figure 9. Left: black hole mass vs. total host galaxy stellar mass for local AGNs with the kernel density estimate (see the text) shown in grayscale. Contour levels are at $(1/2)^n$ times the peak value, where $n = 1-5$. Right: conditional PDF $p(\log M_{\text{BH}} | \log M_{\text{stellar}})$ computed by normalizing the kernel density estimate at each $\log M_{\text{stellar}}$. The middle line indicates the median of the PDF as a function of $\log M_{\text{stellar}}$, and the outer white lines show the standard deviation.

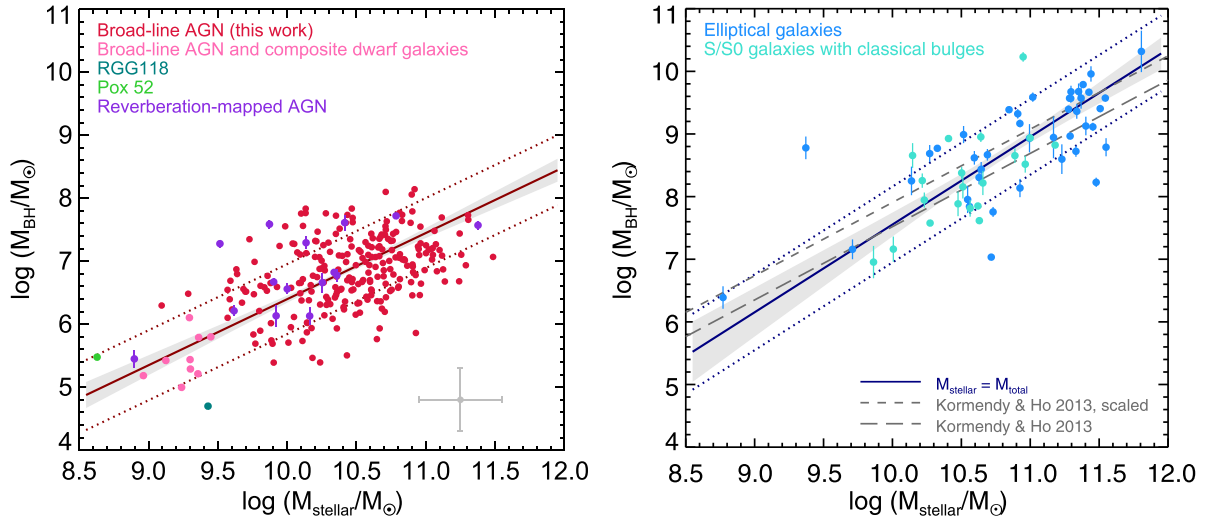


Figure 10. Left: the BH-to-total stellar mass relation for local AGNs (dark red line; Equations (4) and (5)). The light gray shaded region accounts for the errors in the slope and intercept of the relation, and the dark red dotted lines indicate the rms scatter of points around the relation (0.55 dex). The gray error bar indicates uncertainties in stellar masses for all points, and single-epoch spectroscopic BH masses. BH mass errors for the reverberation-mapped AGNs are shown on the (purple) data points. Right: same as the left panel, but for the inactive sample of elliptical galaxies and sprial/S0 galaxies with classical bulges (Equations (4) and (6)). The dark blue line indicates our relation derived using total stellar mass (Section 3.3).

when using only our primary sample of broad-line AGNs (Section 2) and excluding the additional AGNs described in Sections 3.1 and 3.2. The slope and intercept derived from our uniformly selected sample agree with those in Equation (5) within the 1σ uncertainties.

The BH-to-total stellar mass relation for the ellipticals and classical bulges is shown in the right panel of Figure 10 for comparison. The corresponding coefficients in Equation (4) are given by

$$\alpha = 8.95 \pm 0.09; \beta = 1.40 \pm 0.21, \quad (6)$$

and the intrinsic scatter is 0.47 dex (rms = 0.60 dex).

4.2. Implications for BH-to-stellar Mass Fractions

Figure 11 shows BH mass fractions as a function of stellar mass for our two *total* stellar mass relations at $z \sim 0$ (AGNs and dynamically measured BHs; Equations (4)–(6)), as well as some standard BH-to-*bulge* mass relations (e.g., Häring & Rix 2004; Kormendy & Ho 2013; McConnell & Ma 2013). The BH-to-total stellar mass fraction given by the AGN relation is $M_{\text{BH}}/M_{\text{stellar}} \sim 0.02\%–0.03\%$ across the stellar mass range $10^8 \leq M_{\text{stellar}}/M_{\odot} \leq 10^{12}$. This is markedly smaller, by roughly an order of magnitude, than the BH-to-bulge mass fractions derived from quiescent early-type galaxies that are commonly used as references.

For instance, the BH mass fraction given by our AGN total stellar mass relation is $\sim 19–56$ times lower than that given by the canonical BH-to-bulge mass relation of Kormendy & Ho (2013) across the stellar mass range $10^8 \leq M_{\text{stellar}}/M_{\odot} \leq 10^{12}$, accounting for differences in our assumed stellar mass-to-light ratios (see Section 3.3). Using total stellar mass rather than bulge mass for the host galaxies of dynamically measured BHs in ellipticals and classical bulges also results in a BH mass fraction that is roughly an order of magnitude larger than that of the AGN host galaxies. We thus urge extreme caution when using the canonical BH-to-bulge mass scaling relations as a proxy for BH-to-total stellar masses since this may lead to a biased interpretation.

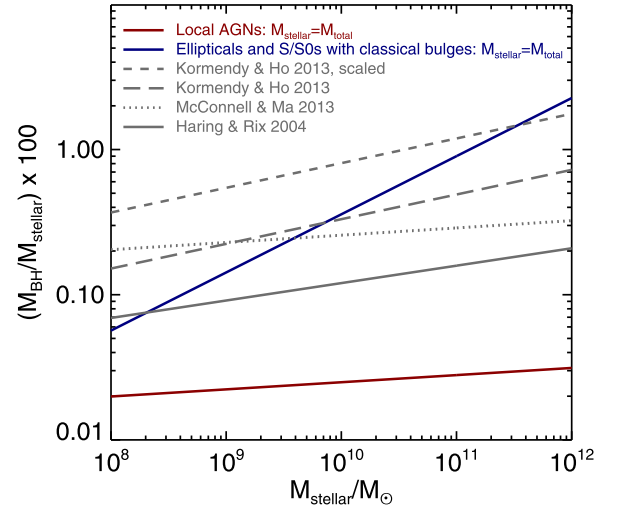


Figure 11. BH mass fractions (given as a percentage of the stellar mass) as a function of stellar mass. Our local AGN relation, where $M_{\text{stellar}} = M_{\text{total}}$, is shown as a dark red line. Our total stellar mass relation for quiescent BHs in early-type galaxies is shown as a dark blue line. Bulge mass relations from the literature are shown as gray lines.

4.3. Systematic Uncertainties

Based on the $z \sim 0$ samples presented in this work, we have shown that AGNs occupy a region in the $\log M_{\text{stellar}} - \log M_{\text{BH}}$ plane below that populated by ellipticals and classical bulges. Here we consider systematic uncertainties in stellar and BH masses that may affect this empirical result. We note that differences in distance scales are negligible. The range of assumed H_0 across all samples represented in Figure 8 varies from 70 to $71 \text{ km s}^{-1} \text{ Mpc}^{-1}$.

We do not expect that systematic uncertainties in stellar masses between the samples shown in Figure 10 can account for the two different relations. First, all stellar masses have been estimated in the most consistent manner feasible. That is, we use color-dependent mass-to-light ratios provided by Zibetti et al. (2009) with either a combination of *g*- and *i*-band SDSS

data (all AGNs except Pox 52) or B -, V -, and K -band data (galaxies with dynamical BH masses and Pox 52). As described in Section 2.4, we have accounted for any AGN contribution when calculating stellar masses, so we do not think AGN host galaxy masses are significantly overestimated. Moreover, in order to bring the sample of AGNs onto the upper relation by shifting their stellar masses, the stellar masses would need to be reduced by more than an order of magnitude (see Figure 8).

The virial BH masses estimated for our sample of broad-line AGNs are quite indirect and subject to various uncertainties. For example, the BLR geometry and orientation certainly varies between objects (Kollatschny 2003; Bentz et al. 2009; Denney et al. 2010; Barth et al. 2011), yet we apply a single geometric scaling factor since we do not have this information for the individual broad-line AGNs in our sample. There is also the possibility that there are nongravitational contributions to the measured gas velocities (e.g., Krolik 2001), although this would lead to systematically overestimated BH masses.

The lower relation defined by the broad-line AGNs has a normalization that is ~ 1.2 dex lower than the upper relation at $M_{\text{stellar}} = 10^{10} M_{\text{sun}}$. Across our sample, uncertainties in the virial BH mass estimates are expected to be on the order of ~ 0.5 dex (e.g., Vestergaard & Peterson 2006; Shen 2013), which is considerably less than the offset in BH mass between the two relations. Any reasonable variation in the virial factor can also be ruled out as producing artificially low BH masses for the broad-line AGNs. In order to get AGN BH masses to fall on the upper relation by changing the virial factor, $\langle f \rangle$ would need to be $\gtrsim 40$ ($\epsilon \gtrsim 10$ in Equation (1)). Finally, we note that dynamically measured BHs in galaxies with pseudobulges, as well as the reverberation-mapped AGNs, overlap our sample of broad-line AGNs. For all of these reasons, we conclude that uncertainties in virial BH masses alone are not artificially producing a lower relation in the $\log M_{\text{stellar}} - \log M_{\text{BH}}$ plane for the AGNs.

We note that we have discarded nine objects from our sample of AGNs in which the luminosity of the AGN dominates the total integrated photometry (host + AGN). Our motivation for this was to minimize unreliable stellar mass estimates. For a fixed stellar mass and Eddington ratio, this could bias us against large $M_{\text{BH}}/M_{\text{stellar}}$. However, given that only $\sim 3\%$ of the AGNs were removed from our sample, we do not think this has impacted our results in any appreciable way.

4.4. Possible Origins for the Separation between AGN Hosts and Ellipticals/Classical Bulges

We now turn our attention to possible origins for two BH-to-total stellar mass relations: one comprising AGNs, the other ellipticals and classical bulges, with pseudobulges predominantly overlapping the AGNs. It is worth noting that at least some of the galaxies with pseudobulges are active because they are selected as being masers. Others, like the Milky Way, are obviously inactive.

Given that the lower relation is defined by AGNs and the upper relation is defined by quiescent BHs with dynamical BH mass measurements, it is reasonable to consider whether nuclear activity (or lack thereof) may be partially responsible for the existence of two separate relations. On the one hand, there are reasons to question the importance of nuclear activity since the samples defining the two relations are each fraught with their own selection biases. Dynamical BH mass measurements are severely biased toward nearby, massive, and dense

galaxies where the BH sphere of influence can be resolved (e.g., van den Bosch et al. 2015). Gültekin et al. (2011) showed that dynamical BH masses are not biased high in the $M_{\text{BH}} - \sigma_*$ plane for very large galaxies ($\langle \sigma_* \rangle \sim 268 \text{ km s}^{-1}$); however, we are probing significantly lower masses. There is no reason that galaxies with quiescent BHs should not overlap with the AGN host galaxies in Figure 8; we just cannot detect such BHs. On the other hand, we see in Figure 8 that we do not detect AGNs with BH masses as large as the quiescent BHs at a given stellar mass, suggesting that nuclear activity is an important factor. If there were AGNs with such large BH masses, we should see them because they would be bright. Apparently, the larger BHs (at a given stellar mass) are not shining as AGNs (see also, e.g., Heckman et al. 2004; Merloni 2004).

Another potential factor is differences in host galaxy properties. A comparison of the Hubble types of galaxies with dynamically detected BHs (from Kormendy & Ho 2013) supports this notion. For example, the classical bulges are mostly hosted by early-type S0 galaxies (16/20 have Hubble types of S0 or SB0), and they overlap with the elliptical galaxies. Alternatively, the pseudobulges that tend to overlap with the AGN host galaxies are more commonly found in later-type spiral galaxies (2/17 are found in SB0 galaxies; the rest are in spirals).

We find that a significant fraction of local broad-line AGN host galaxies are also spirals/disks, similar to what has previously been found in studies of moderate-luminosity AGN host galaxies out to $z \sim 3$ (e.g., Gabor et al. 2009; Schawinski et al. 2011; Kocevski et al. 2012; Bennert et al. 2015). We obtained approximate Hubble types for a subset of the AGN host galaxies using automated morphological classifications from Huertas-Company et al. (2011). The automated classifications from this work have been shown to correlate well with visual classifications. Rather than assigning a single morphological classification, Huertas-Company et al. (2011) provide probabilities of being in four morphological classes (E, S0, Sab, Scd). For the AGN host galaxies with matches in the Huertas-Company et al. (2011) catalog (129 objects), we simply adopt the class with the highest probability.

In Figure 12, we plot $\log M_{\text{BH}}$ versus $\log M_{\text{stellar}}$ with points color-coded by morphological class. We also include the galaxies with dynamical BH masses, converting Hubble types provided by Kormendy & Ho (2013) to either E, S0, Sab, or Scd. Based on these rough morphological classifications, it is clear that a significantly higher fraction of spiral galaxies lies close to the lower relation compared to the upper relation. These spiral galaxies will have less prominent bulges than the galaxies on the upper relation, which are mostly bulge-dominated elliptical and S0 galaxies.

The AGN host galaxies on the lower BH-to-total stellar mass relation could conceivably follow the canonical BH-to-bulge mass relation⁹ if the classical bulge masses for the AGN hosts were, on average, only $\sim 5\%$ of the total stellar masses. This echoes the result of the model for bulge evolution by Lu & Mo (2015), where their reference model (Model III) is a very good fit to our data. Sanghvi et al. (2014) also find that low-mass quasars lie below the extrapolation of the local BH-to-bulge mass relation, but with a correction for the disk they obey it. Caplar et al. (2015) advocate a lower $M_{\text{BH}}/M_{\text{stellar}}$ ratio for

⁹ We have scaled the BH-to-bulge mass relation of Kormendy & Ho (2013) to account for our different assumed stellar mass-to-light ratios as discussed in Section 3.3.

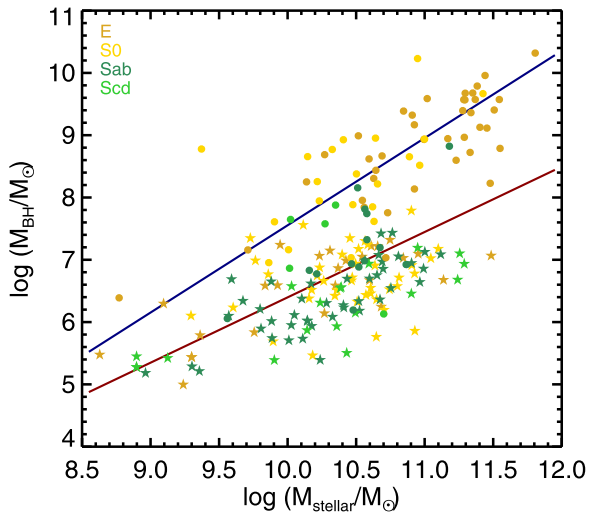


Figure 12. Log M_{BH} vs. log M_{stellar} with points color-coded by approximate morphological type (see the text in Section 4.4). AGNs are plotted as stars, and dynamically detected BHs are plotted as circles. The dark red line indicates our BH-to-total stellar mass relation based on local AGNs (Equations (4) and (5)). The dark blue line indicates our BH-to-total stellar mass relation based on ellipticals and galaxies with classical bulges hosting dynamically detected BHs (Equations (4) and (6)).

local active galaxies compared to inactive galaxies that have “quenched” at earlier times.

5. CONCLUSIONS AND DISCUSSION

In this paper, we have studied the relation between BH mass and total stellar mass for nearby galaxies ($z < 0.055$), including both galaxies with inactive BHs, with dynamical BH mass measurements, and galaxies with an active BH, with mass measurements based on reverberation mapping or single-epoch virial estimates. Inclusion of the latter sources allows us to extend our sample to low BH masses, and also to use the same technique used at higher redshift. Moreover, our stellar mass measurements rely on mass-to-light ratios, as is routinely the case for higher-redshift samples. Therefore we build a local analog of higher-redshift samples, but where we have better control of systematics. Our work is complementary to Läscher et al. (2014), where they measure in a uniform way the total luminosities of a sample of galaxies with dynamically measured BHs, in that we try to provide a benchmark for observational or theoretical studies where detailed information on bulge properties is not available. Bennert et al. (2015) also took a similar approach toward the correlation with velocity dispersion. One important caveat in our analysis is that the AGNs we have studied are moderate-luminosity Seyferts ($41.5 \lesssim \log L_{\text{bol}} \lesssim 44.4$). At high-redshift, statistical samples are often biased toward more luminous AGNs and quasars.

In Figure 8, we plot BH mass versus total stellar mass for galaxies with $10^{8.5} \lesssim M_{\text{stellar}} \lesssim 10^{12} M_{\odot}$. A single linear fit to the data is disfavored. Rather, the AGN host galaxies define a relation that has a similar slope ($M_{\text{BH}} \propto M_{\text{stellar}}$) to early-type galaxies with quiescent BHs, but a normalization that is more than an order of magnitude lower (Figures 10 and 11). The different normalizations may be partially due to active versus inactive BHs, but can also be attributed to differences in host galaxy (bulge) properties as discussed in Section 4.4. We caution that using the $z = 0$ benchmark BH-to-bulge mass relations for AGN host galaxies, or assuming $M_{\text{bulge}} = M_{\text{total}}$,

may lead to severely biased interpretations. For example, Graham & Scott (2015) assume that bulge mass equals total stellar mass for the 10 broad-line AGNs and composite dwarf galaxies in Reines et al. (2013), which in part leads them to conclude that AGN host galaxies follow a steeper, quadratic-like relation between BH mass and bulge mass.

Our work also has important implications for cosmological simulations that are tied to the local BH-to-bulge mass relations. In most cosmological simulations that produce statistical samples of BHs and AGNs, i.e., large uniform-volume simulations (e.g., MassiveBlack I and II, Di Matteo et al. 2012; DeGraf et al. 2014; Illustris, Sijacki et al. 2015; Eagle, Schaye et al. 2015; Horizon-AGN, Dubois et al. 2014), the resolution is limited to approximately kiloparsec scales, making bulge-disk decomposition for low-mass galaxies unreliable. The typical approach, in fact, is to estimate the total stellar mass within the stellar half-mass-radius (Sijacki et al. 2015) or twice that (DeGraf et al. 2014), or extrapolate a fit to the mass profile of the bulge inferred from kinematic data (Schaye et al. 2015). If the simulations do not select ellipticals or galaxies with classical bulges and perform a bulge-disk decomposition, using the relations published in the literature for BH-bulge mass (e.g., Marconi & Hunt 2003; Häring & Rix 2004; Kormendy & Ho 2013; McConnell & Ma 2013) as a benchmark for the comparison between simulations and observations at $z = 0$ (and perhaps beyond) would not be appropriate. Our method is easier to implement in the analysis of simulations and can help disentangle issues related to BH growth and AGN properties.

Whether or not the BH-to-total stellar mass relation extends to even smaller masses bears directly to the origin of BH “seeds.” Volonteri & Natarajan (2009) and van Wassenhove et al. (2010) suggested that if BH seeds are massive, e.g., $10^5 M_{\odot}$, as predicted by “direct collapse” models, the low-mass end of the relation between BHs and galaxies (they specifically referred to the correlation with the velocity dispersion, but the result would hold for the stellar mass as well) flattens toward an asymptotic value, creating a characteristic “plume” of ungrown BHs. Vice versa, if BH seeds are small, e.g., $10^2 M_{\odot}$, as predicted by models related to the first generation of stars, the expectation is that the observable scaling laws would not see the asymptotic value (the “plume”) because it lies at masses below those that can be probed observationally.

Finally, extending the sample at stellar masses $\sim 10^9 M_{\odot}$ is fundamental to interpret results for much higher redshift galaxies with similar masses. Searches for AGNs in galaxies with stellar masses $\sim 10^9 M_{\odot}$ at $z > 6$ have found very few, if any, BHs (Willott 2011; Cowie et al. 2012; Fiore et al. 2012; Treister et al. 2013; Giallongo et al. 2015; Weigel et al. 2015). If our sample is a good representation of the local universe, and the same relation based on local AGNs holds at high redshift, it explains why we do not easily detect BHs at high z : their masses would lie below the extrapolation of the local BH-bulge mass relation, which is normally used as a benchmark. Volonteri & Stark (2011) suggested that observations could indeed be explained with a BH-stellar mass correlation either steeper than at $z = 0$ or with a lower normalization. Dubois et al. (2015) suggest that the growth of BHs in low-mass galaxies (galaxy mass $< 10^{10} M_{\odot}$ and bulge mass $< 10^9 M_{\odot}$) is stunted because of supernova feedback, which hinders accumulation of gas in the nucleus until the potential well of the bulge and galaxy become deep enough. In forthcoming work, we will explore the

consequences of our results on the interpretation of high- z BH populations, and the link to their hosts.

It is our pleasure to thank Rich Plotkin, Eric Bell, Kayhan Gültekin, and Jenny Greene for very helpful discussions. We also thank the anonymous referee for useful comments and suggestions. Support for AER was provided by NASA through Hubble Fellowship grant HST-HF2-51347.001-A awarded by the Space Telescope Science Institute, which is operated by the Association of Universities for Research in Astronomy, Inc., for NASA, under contract NAS 5-26555. M.V. acknowledges funding from the European Research Council under the European Community's Seventh Framework Programme (FP7/2007-2013 grant agreement No. 614199, project "BLACK").

REFERENCES

- Aihara, H., Allende Prieto, C., An, D., et al. 2011, *ApJS*, 193, 29
- Baldassare, V. F., Reines, A. E., Gallo, E., & Greene, J. E. 2015, *ApJL*, 809, L14
- Baldwin, J. A., Phillips, M. M., & Terlevich, R. 1981, *PASP*, 93, 5
- Barth, A. J., Ho, L. C., Rutledge, R. E., & Sargent, W. L. W. 2004, *ApJ*, 607, 90
- Barth, A. J., Pancoast, A., Thorman, S. J., et al. 2011, *ApJL*, 743, L4
- Beifiori, A., Courteau, S., Corsini, E. M., & Zhu, Y. 2012, *MNRAS*, 419, 2497
- Bell, E. F., & de Jong, R. S. 2001, *ApJ*, 550, 212
- Bell, E. F., McIntosh, D. H., Katz, N., & Weinberg, M. D. 2003, *ApJS*, 149, 289
- Bennert, V. N., Treu, T., Auger, M. W., et al. 2015, *ApJ*, 809, 20
- Bentz, M. C., Denney, K. D., Grier, C. J., et al. 2013, *ApJ*, 767, 149
- Bentz, M. C., & Katz, S. 2015, *PASP*, 127, 67
- Bentz, M. C., Walsh, J. L., Barth, A. J., et al. 2009, *ApJ*, 705, 199
- Blanton, M. R., Kazin, E., Muna, D., Weaver, B. A., & Price-Whelan, A. 2011, *AJ*, 142, 31
- Blanton, M. R., & Roweis, S. 2007, *AJ*, 133, 734
- Bongiorno, A., Maiolino, R., Brusa, M., et al. 2014, *MNRAS*, 443, 2077
- Caplar, N., Lilly, S. J., & Trakhtenbrot, B. 2015, arXiv:1411.3719
- Cisternas, M., Jahnke, K., Bongiorno, A., et al. 2011, *ApJL*, 741, L11
- Conroy, C., Gunn, J. E., & White, M. 2009, *ApJ*, 699, 486
- Cowie, L. L., Barger, A. J., & Hasinger, G. 2012, *ApJ*, 748, 50
- Decarli, R., Falomo, R., Treves, A., et al. 2010, *MNRAS*, 402, 2453
- DeGraf, C., Di Matteo, T., Treu, T., et al. 2014, arXiv:1412.4133
- Denney, K. D., Peterson, B. M., Pogge, R. W., et al. 2010, *ApJ*, 721, 715
- Di Matteo, T., Khandai, N., DeGraf, C., et al. 2012, *ApJL*, 745, L29
- Dong, X., Wang, T., Yuan, W., et al. 2007, *ApJ*, 657, 700
- Dubois, Y., Pichon, C., Welker, C., et al. 2014, *MNRAS*, 444, 1453
- Dubois, Y., Volonteri, M., Silk, J., et al. 2015, *MNRAS*, 452, 1502
- Ferrarese, L., & Merritt, D. 2000, *ApJL*, 539, L9
- Ferrarese, L., Pogge, R. W., Peterson, B. M., et al. 2001, *ApJL*, 555, L79
- Filippenko, A. V., & Ho, L. C. 2003, *ApJL*, 588, L13
- Filippenko, A. V., & Sargent, W. L. W. 1989, *ApJL*, 342, L11
- Fiore, F., Puccetti, S., Grazian, A., et al. 2012, *A&A*, 537, A16
- Gabor, J. M., Impey, C. D., Jahnke, K., et al. 2009, *ApJ*, 691, 705
- Gallazzi, A., Brinchmann, J., Charlot, S., & White, S. D. M. 2008, *MNRAS*, 383, 1439
- Gebhardt, K., Bender, R., Bower, G., et al. 2000a, *ApJL*, 539, L13
- Gebhardt, K., Kormendy, J., Ho, L. C., et al. 2000b, *ApJL*, 543, L5
- Giallongo, E., Grazian, A., Fiore, F., et al. 2015, *A&A*, 578, A83
- Graham, A. W., & Scott, N. 2015, *ApJ*, 798, 54
- Greene, J. E., & Ho, L. C. 2005, *ApJ*, 630, 122
- Greene, J. E., & Ho, L. C. 2006, *ApJL*, 641, L21
- Greene, J. E., & Ho, L. C. 2007a, *ApJ*, 670, 92
- Greene, J. E., & Ho, L. C. 2007b, *ApJ*, 667, 131
- Greene, J. E., Peng, C. Y., Kim, M., et al. 2010, *ApJ*, 721, 26
- Grier, C. J., Martini, P., Watson, L. C., et al. 2013, *ApJ*, 773, 90
- Groves, B. A., Heckman, T. M., & Kauffmann, G. 2006, *MNRAS*, 371, 1559
- Gültekin, K., Richstone, D. O., Gebhardt, K., et al. 2009, *ApJ*, 698, 198
- Gültekin, K., Tremaine, S., Loeb, A., & Richstone, D. O. 2011, *ApJ*, 738, 17
- Håring, N., & Rix, H.-W. 2004, *ApJL*, 604, L89
- Heckman, T. M., Kauffmann, G., Brinchmann, J., et al. 2004, *ApJ*, 613, 109
- Ho, L. C., & Kim, M. 2014, *ApJ*, 789, 17
- Huertas-Company, M., Aguerri, J. A. L., Bernardi, M., Mei, S., & Sánchez Almeida, J. 2011, *A&A*, 525, A157
- Into, T., & Portinari, L. 2013, *MNRAS*, 430, 2715
- Jahnke, K., Bongiorno, A., Brusa, M., et al. 2009, *ApJL*, 706, L215
- Kaspi, S., Maoz, D., Netzer, H., et al. 2005, *ApJ*, 629, 61
- Kauffmann, G., Heckman, T. M., Tremonti, C., et al. 2003, *MNRAS*, 346, 1055
- Kelly, B. C. 2007, *ApJ*, 665, 1489
- Kelly, B. C., & Merloni, A. 2012, *AdAst*, 2012, 970858
- Kewley, L. J., Dopita, M. A., Leitherer, C., et al. 2013, *ApJ*, 774, 100
- Kewley, L. J., Dopita, M. A., Sutherland, R. S., Heisler, C. A., & Trevena, J. 2001, *ApJ*, 556, 121
- Kewley, L. J., Groves, B., Kauffmann, G., & Heckman, T. 2006, *MNRAS*, 372, 961
- Kocevski, D. D., Faber, S. M., Mozena, M., et al. 2012, *ApJ*, 744, 148
- Kollatschny, W. 2003, *A&A*, 407, 461
- Kormendy, J., Bender, R., & Cornell, M. E. 2011, *Natur*, 469, 374
- Kormendy, J., & Ho, L. C. 2013, *ARA&A*, 51, 511
- Krolik, J. H. 2001, *ApJ*, 551, 72
- Läsker, R., Ferrarese, L., van de Ven, G., & Shankar, F. 2014, *ApJ*, 780, 70
- Lauer, T. R., Tremaine, S., Richstone, D., & Faber, S. M. 2007, *ApJ*, 670, 249
- Lu, Z., & Mo, H. J. 2015, *ApJ*, 802, 110
- Magorrian, J., Tremaine, S., Richstone, D., et al. 1998, *AJ*, 115, 2285
- Marconi, A., & Hunt, L. K. 2003, *ApJL*, 589, L21
- Marconi, A., Risaliti, G., Gilli, R., et al. 2004, *MNRAS*, 351, 169
- McConnell, N. J., & Ma, C.-P. 2013, *ApJ*, 764, 184
- Merloni, A. 2004, *MNRAS*, 353, 1035
- Merloni, A. E. A. 2010, *ApJ*, 708, 137
- Nelson, C. H., Green, R. F., Bower, G., Gebhardt, K., & Weistrop, D. 2004, *ApJ*, 615, 652
- Onken, C. A., Ferrarese, L., Merritt, D., et al. 2004, *ApJ*, 615, 645
- Park, D., Woo, J.-H., Bennert, V. N., et al. 2015, *ApJ*, 799, 164
- Park, D., Woo, J.-H., Treu, T., et al. 2012, *ApJ*, 747, 30
- Peng, C. Y., Impey, C. D., Rix, H.-W., et al. 2006, *ApJ*, 649, 616
- Peterson, B. M., Ferrarese, L., Gilbert, K. M., et al. 2004, *ApJ*, 613, 682
- Reines, A. E., & Deller, A. T. 2012, *ApJL*, 750, L24
- Reines, A. E., Greene, J. E., & Geha, M. 2013, *ApJ*, 775, 116
- Reines, A. E., Plotkin, R. M., Russell, T. D., et al. 2014, *ApJL*, 787, L30
- Reines, A. E., Sivakoff, G. R., Johnson, K. E., & Brogan, C. L. 2011, *Natur*, 470, 66
- Richards, G. T., Lacy, M., Storrie-Lombardi, L. J., et al. 2006, *ApJS*, 166, 470
- Sanghi, J., Kotilainen, J. K., Falomo, R., et al. 2014, *MNRAS*, 445, 1261
- Schawinski, K., Treister, E., Urry, C. M., et al. 2011, *ApJL*, 727, L31
- Schaye, J., Crain, R. A., Bower, R. G., et al. 2015, *MNRAS*, 446, 521
- Schlegel, D. J., Finkbeiner, D. P., & Davis, M. 1998, *ApJ*, 500, 525
- Schramm, M., & Silverman, J. D. 2013, *ApJ*, 767, 13
- Schulze, A., & Wisotzki, L. 2010, *A&A*, 516, A87
- Secrest, N. J., Satyapal, S., Gliozzi, M., et al. 2015, *ApJ*, 798, 38
- Shankar, F., Salucci, P., Granato, G. L., De Zotti, G., & Danese, L. 2004, *MNRAS*, 354, 1020
- Shankar, F., Weinberg, D. H., & Miralda-Escudé, J. 2009, *ApJ*, 690, 20
- Shen, Y. 2013, *BASI*, 41, 61
- Sijacki, D., Vogelsberger, M., Genel, S., et al. 2015, *MNRAS*, 452, 575
- Silverman, B. W. 1986, *Monographs on Statistics and Applied Probability* (London: Chapman and Hall)
- Sun, M., Trump, J. R., Brandt, W. N., et al. 2015, *ApJ*, 802, 14
- Targett, T. A., Dunlop, J. S., & McLure, R. J. 2012, *MNRAS*, 420, 3621
- Thornton, C. E., Barth, A. J., Ho, L. C., Rutledge, R. E., & Greene, J. E. 2008, *ApJ*, 686, 892
- Treister, E., Schawinski, K., Volonteri, M., & Natarajan, P. 2013, *ApJ*, 778, 130
- Vanden Berk, D. E., Richards, G. T., Bauer, A., et al. 2001, *AJ*, 122, 549
- van den Bosch, R. C. E., Gebhardt, K., Gültekin, K., Yıldırım, A., & Walsh, J. L. 2015, *ApJS*, 218, 10
- van Wassenhove, S., Volonteri, M., Walker, M. G., & Gair, J. R. 2010, *MNRAS*, 408, 1139
- Veilleux, S., & Osterbrock, D. E. 1987, *ApJS*, 63, 295
- Vestergaard, M., & Osmer, P. S. 2009, *ApJ*, 699, 800
- Vestergaard, M., & Peterson, B. M. 2006, *ApJ*, 641, 689
- Volonteri, M., & Natarajan, P. 2009, *MNRAS*, 400, 1911
- Volonteri, M., & Stark, D. P. 2011, *MNRAS*, 417, 2085
- Weigel, A. K., Schawinski, K., Treister, E., et al. 2015, *MNRAS*, 448, 3167
- Willcock, J. A., Courteau, S., Faber, S. M., et al. 1997, *ApJS*, 109, 333
- Willott, C. J. 2011, *ApJL*, 742, L8
- Yan, R. 2011, *AJ*, 142, 153
- Yan, R., & Blanton, M. R. 2012, *ApJ*, 747, 61
- Zibetti, S., Charlot, S., & Rix, H.-W. 2009, *MNRAS*, 400, 1181